



OPEN ACCESS

EDITED BY

Zuzana Macek Jilkova,
Centre Hospitalier Universitaire de
Grenoble, France

REVIEWED BY

Xuan Wu,
Zhengzhou University, China
Gabriele Multhoff,
Technical University of Munich, Germany
Pardeep Kumar,
National Institute of Mental Health and
Neurosciences, India
Weijun Wei,
School of Medicine, Shanghai Jiao Tong
University, China

*CORRESPONDENCE

Ignacio Gil-Bazo
✉ igbazo@fivo.org

†PRESENT ADDRESS

Ignacio Gil-Bazo,
Fundación Instituto Valenciano de
Oncología, Valencia, Spain

RECEIVED 04 August 2023

ACCEPTED 12 September 2023

PUBLISHED 28 September 2023

CITATION

Puyalto A, Rodríguez-Remírez M, López I,
Iribarren F, Simón JA, Ecay M, Collantes M,
Vilalta-Lacarra A, Francisco-Cruz A,
Solórzano JL, Sandiego S, Peñuelas I,
Calvo A, Ajona D and Gil-Bazo I (2023)
A novel [⁸⁹Zr]-anti-PD-1-PET-CT to
assess response to PD-1/PD-L1
blockade in lung cancer.
Front. Immunol. 14:1272570.
doi: 10.3389/fimmu.2023.1272570

COPYRIGHT

© 2023 Puyalto, Rodríguez-Remírez, López,
Iribarren, Simón, Ecay, Collantes,
Vilalta-Lacarra, Francisco-Cruz, Solórzano,
Sandiego, Peñuelas, Calvo, Ajona and
Gil-Bazo. This is an open-access article
distributed under the terms of the [Creative
Commons Attribution License \(CC BY\)](https://creativecommons.org/licenses/by/4.0/). The
use, distribution or reproduction in other
forums is permitted, provided the original
author(s) and the copyright owner(s) are
credited and that the original publication in
this journal is cited, in accordance with
accepted academic practice. No use,
distribution or reproduction is permitted
which does not comply with these terms.

A novel [⁸⁹Zr]-anti-PD-1-PET-CT to assess response to PD-1/PD-L1 blockade in lung cancer

Ander Puyalto^{1,2,3}, María Rodríguez-Remírez^{1,2,3}, Inés López^{2,3},
Fabiola Iribarren^{1,2}, Jon Ander Simón^{2,4,5}, Marga Ecay^{4,5},
María Collantes^{4,5}, Anna Vilalta-Lacarra^{1,2},
Alejandro Francisco-Cruz⁶, Jose Luis Solórzano^{7,8},
Sergio Sandiego⁹, Iván Peñuelas^{3,4,5}, Alfonso Calvo^{2,3,10},
Daniel Ajona^{2,3,10} and Ignacio Gil-Bazo^{1,2,3,9,10*†}

¹Department of Medical Oncology, Clínica Universidad de Navarra, Pamplona, Spain, ²University of Navarra, Cima-University of Navarra, Program in Solid Tumors, Pamplona, Spain, ³Instituto de Investigación Sanitaria de Navarra (IDISNA), Pamplona, Spain, ⁴Department of Nuclear Medicine, Clínica Universidad de Navarra, Pamplona, Spain, ⁵Translational Molecular Imaging Unit, Clínica Universidad de Navarra, Pamplona, Spain, ⁶Department of Pathology, National Institute of Cardiology Ignacio Chavez, Mexico City, Mexico, ⁷Departamento de Anatomía Patológica y Diagnóstico Molecular, Md Anderson Cancer Center, Madrid, Spain, ⁸Unidad de Investigación Clínica de Cáncer de Pulmón Hospital Universitario 12 de octubre- Centro Nacional de Investigaciones Oncológicas (H12O-CNIO), Madrid, Spain, ⁹Department of Oncology, Fundación Instituto Valenciano de Oncología (FIVO), Valencia, Spain, ¹⁰Centro de Investigación Biomédica en Red - Cáncer (CIBERONC), Madrid, Spain

Background: Harnessing the anti-tumor immune system response by targeting the program cell death protein (PD-1) and program cell death ligand protein (PD-L1) axis has been a major breakthrough in non-small cell lung cancer (NSCLC) therapy. Nonetheless, conventional imaging tools cannot accurately assess response in immunotherapy-treated patients. Using a lung cancer syngeneic mouse model responder to immunotherapy, we aimed to demonstrate that [⁸⁹Zr]-anti-PD-1 immuno-PET is a safe and feasible imaging modality to assess the response to PD-1/PD-L1 blockade in NSCLC.

Materials and methods: A syngeneic mouse model responder to anti-PD-1 therapy was used. Tumor growth and response to PD-1 blockade were monitored by conventional 2-deoxy-2-[¹⁸F]fluoro-D-glucose ([¹⁸F]-FDG) PET scans. Additionally, tumor lymphocyte infiltration was analyzed by the use of an [⁸⁹Zr]-labeled anti-PD-1 antibody and measured as ⁸⁹Zr tumor uptake.

Results: Conventional [¹⁸F]-FDG-PET scans failed to detect the antitumor activity exerted by anti-PD-1 therapy. However, [⁸⁹Zr]-anti-PD-1 uptake was substantially higher in mice that responded to PD-1 blockade. The analysis of tumor-infiltrating immune cell populations and interleukins demonstrated an increased anti-tumor effect elicited by activation of effector immune cells in PD-1-responder mice. Interestingly, a positive correlation between [⁸⁹Zr]-anti-PD-1 uptake and the proportion of tumor-infiltrating lymphocytes (TILs) was found ($Cor = 0.8$; $p = 0.001$).

Conclusion: Our data may support the clinical implementation of immuno-PET as a promising novel imaging tool to predict and assess the response of PD-1/PD-L1 inhibitors in patients with NSCLC.

KEYWORDS

lung adenocarcinoma, inhibitor of differentiation 1, PD-1 inhibition, immuno-PET, pseudoprogression

Introduction

Lung cancer is the leading cause of cancer deaths (1). Over the last two decades, the development of targeted therapies against certain oncogenic drivers first, and more recently, the use of immune check-point inhibitors (ICIs) have significantly improved the outcomes of metastatic non-small cell lung cancer (NSCLC) patients (2, 3). More specifically, immune modulation through the blockade of the program cell death protein (PD-1)/program cell death ligand protein (PD-L1) axis has obtained the best long-term survival rates ever, with more than 30% of patients being alive at five years (4). ICIs, such as PD-1/PD-L1 monoclonal antibodies (mAbs), reactivate the antigen-specific effector T cells, thus boosting the anti-tumor immune response. Nevertheless, tumor response assessment has become a challenge in NSCLC patients receiving immunotherapy-based systemic regimens.

Although immunohistochemical PD-L1 expression in NSCLC is a predictive biomarker of response to PD-1/PD-L1-inhibiting mAbs, other potential predictive biomarkers such as PD-1 expression in tumor-infiltrating lymphocytes (TILs) or the ability of the PD-1 antibody to reach its target have not been evaluated (5). Moreover, the discovery of new combination therapies are emerging to further improve the efficacy of ICIs (6). Recent reports have demonstrated how targeted therapies can modulate the antigenicity of tumor cells and enhance T cell immune recognition, resulting in a potentially synergistic improvement of the efficacy of this therapeutic approach (7, 8).

Inhibitor of differentiation-1 (*Id1*) is a negative transcription regulator that belongs to the *Id* (*Id1-Id4*) gene family (9, 10). In NSCLC patients, *Id1* has been associated with poor response and prognosis, as it plays a central role in tumorigenesis, tumor angiogenesis, metastasis, and tumor progression, suppressing the antitumor immune response (11–14). Moreover, *Id1* has been described as an immunosuppressor factor involved in the generation of an immunosuppressive tumor microenvironment during tumor progression. In advanced melanoma, *Id1* upregulation through tumor growth factor β (TGF- β) has been shown to promote the differentiation of dendritic cells (DCs) to myeloid-derived suppressor cells (MDSCs) and to suppress CD8⁺ T-cell proliferation (12). Furthermore, a recent analysis of *Id1* expression from peripheral blood mononuclear cells of stage III and IV melanoma patients, strongly associates high *Id1* levels with the presence of phenotypic and immunosuppressive markers in monocytic MDSCs, whereas low *Id1* levels are associated with a

more immunogenic myeloid phenotype (15). More recently, our group has shown that the combined blockade of *Id1* and PD-1/PD-L1 displays synergistic therapeutic activity in *KRAS*-mutant lung cancer in mouse models. *Id1* downregulation enhanced PD-L1 expression on lung cancer cells surface and increased CD8⁺ T cell infiltration, sensitizing lung tumors that do not respond to PD-1/PD-L1 mAbs (16). Interestingly, we have also demonstrated how a MEK1/2 inhibitor can modulate the immunosuppressive tumor microenvironment of *KRAS*-mutant lung adenocarcinoma (LUAD) tumors through *Id1* downregulation (unpublished data).

Advanced imaging methods, specifically computed tomography (CT), positron-emission tomography (PET) and magnetic resonance imaging (MRI), have been established as powerful tools for the staging of lung cancer and the accurate assessment of therapeutic response (17, 18). PET is a well-established 3-dimensional molecular imaging platform that enables non-invasive quantification of the relevant biologic tumor characteristics, using isotope-labelled tracers (19). In NSCLC, the conventional use of 2-deoxy-2-[¹⁸F]fluoro-D-glucose ([¹⁸F]-FDG) PET is useful for proper initial staging and response monitoring of patients on systemic treatment. However, this imaging tool may be suboptimal in immunotherapy-treated patients in whom a metabolic uptake increase does not necessarily mean disease progression (20). Response to ICIs is characterized by different patterns, such as progression prior to treatment response (pseudoprogression), hyperprogression, and dissociated responses following treatment. These patterns, however, are not reflected in the Response Evaluation Criteria in Solid Tumors version 1.1 (RECIST 1.1), which is standard for response assessment in oncology. As such, new response evaluation tools are required.

The use of radiotracers other than [¹⁸F]-FDG is emerging as a non-invasive method to monitor in real time the immune landscape of patients receiving ICIs. This approach is currently under evaluation and may potentially enter routine clinical practice if proven effective (21). Monoclonal antibody-based PET (immuno-PET) is another potential biomarker to 1) verify optimal delivery of targeted agents to tumors and, 2) measure target expression (22, 23).

On these premises, we created an *in vivo* immuno-PET model to profile the immune landscape in a lung cancer mouse model exposed to PD-1/PD-L1 axis blockade. Here we provide key evidence on the preclinical implementation of immuno-PET as a novel imaging tool that may detect antitumor effector immune cells. This strategy could be used to predict and assess the response of PD-1/PD-L1 inhibitors in patients with lung cancer.

Materials and methods

Cell lines and reagents

Murine LUAD cell line Lewis lung carcinoma (LLC) was purchased from the American Type Culture Collection (ATCC, Manassas, VA, USA). Cells were cultured in RPMI 1640 medium (Gibco, Waltham, MA, USA) supplemented with 10% fetal bovine serum (FBS) (ThermoFisher, Waltham, MA, USA), 1% penicillin-streptomycin (Gibco, Waltham, MA, USA) and HEPES (Lonza, Basel, Switzerland) and routinely tested for *Mycoplasma* using MycoAlert Mycoplasma Detection Kit (Lonza, Basel, Switzerland). Lentiviral production of shRNA against *Id1* (TRCN0000071436; ThermoFisher, Waltham, MA, USA) was performed as previously described (13, 16). pLKO.1-scramble (pLKO-Scplasmid #1864, Addgene, Watertown, MA, USA) was used as control.

Gene expression

Quantification of interleukins: *interleukin-1 β* (*Il-1 β*); *tumor necrosis factor alpha* (*Tnf- α*) and *interferon gamma* (*Ifn- γ*) gene expression was determined by real-time quantitative PCR as previously described (13, 16). *Gapdh* was used as an endogenous control. The primers designed for RT-PCR are listed in Table S1.

Murine models

All animal procedures were approved by the institutional Committee on Animal Research and Ethics (regional Government of Navarra) under the protocol number CEEA 054-19E1.

This study included 8–12-week-old female C57BL/6J mice (*Id1*^{+/+}) (The Jackson Laboratory, Bar Harbor, ME, USA), and *Id1*-deficient (*Id1*^{-/-} or IDKO) mice with C57BL/6J background. *Id1*^{-/-} mice were kindly provided by Dr. Robert Benezra (Memorial Sloan-Kettering Cancer Center, New York, NY, USA).

Murine LLC cells (1.5×10^6) with constitutive *Id1* expression (LLC- pLKO-Sc) or *Id1*-silenced (LLC-sh-Id1) cells were injected subcutaneously in the flank of C57BL/6J (*Id1*^{+/+} and *Id1*^{-/-}) mice. Tumor-bearing mice were treated with DPBS or anti-PD-1 monoclonal antibody (RMP1-14, BioXCell, Lebanon, NH, USA) 7, 10 and 14 days after cell inoculation [100 μ g per mouse, intraperitoneally (i.p.)]. In the active treatment group, the last injection (day 14) consisted of the anti-PD-1 antibody radiolabeled with zirconium-89 (⁸⁹Zr]-anti-PD-1). Tumors were measured periodically using a digital caliper (DIN862, Ref 112-G, SESA Tools, Hernani, Spain), and tumor volume was calculated using the formula: volume = $\pi/6 \times \text{length} \times \text{width}^2$. At the end of the experiment tumors were harvested and fixed in 4% formaldehyde (pH = 7) for immunohistochemical analyses (Panreac, Castellar del Valles, Spain).

Antibody conjugation and zirconium-89 radiolabeling

Antibody radiolabeling with zirconium-89 was carried out using a slightly modified version of the protocol described by Vosjan MJ (24). Briefly, a buffer exchange was performed in a small fraction of the monoclonal antibody with a 0.1M bicarbonate buffer (pH = 9), which was then incubated with a 3-fold molar excess of the chelator deferoxamine (DFO) dissolved in 20 μ L of dimethyl sulfoxide (Sigma-Aldrich, Saint Louis, MO, USA). After 30 minutes of conjugation, the reaction mixture was purified using a disposable PD-10 desalting column (Healthcare Life Sciences, Eching, Germany). Then 111 MBq of zirconium-89 was added to the anti-PD-1 (RMP1-14, BioXCell, Lebanon, NH, USA) antibody solution (buffered at pH = 7 with HEPES [Lonza, Basel, Switzerland], oxalic acid and sodium bicarbonate) and the reaction was left at room temperature for 30 minutes. Finally, the solution was purified to eliminate any possible non-chelated zirconium-89 by purification with a PD10 column (Healthcare Life Sciences, Eching, Germany).

In vivo PET imaging with [¹⁸F]-FDG and [⁸⁹Zr]-anti-PD-1

All PET images were acquired on a Mosaic (Philips, Amsterdam, The Netherlands) small animal dedicated tomograph and reconstructed applying dead time, decay, random and scattering corrections into a 128 \times 128 matrix with a 1 mm voxel size. Additionally, on the days that [⁸⁹Zr]-anti-PD1 images were acquired, CT images were performed in a U-SPECT6/E-class (MILabs, Duwboot, The Netherlands) system to obtain the corresponding anatomical correlate of the tumors.

To obtain PET [¹⁸F]-FDG images, mice were fasted overnight with *ad libitum* access to drinking water. On the day of the study, a dose of 9.3 ± 0.8 MBq was injected intravenously in the tail vein. After 50 minutes, the animals were anesthetized with 2% isoflurane in 100% O₂ gas and placed prone on the scanner bed for a 15-minute image acquisition. Images with [⁸⁹Zr]-anti-PD-1 were acquired during 30 minutes and 24, 72 and 144 hours post-injection of an intravenous single dose (3.8 ± 0.02 MBq).

PET data were exported and analyzed using the PMOD software (PMOD Technologies Ltd., Adliswil, Switzerland) and transformed to standardized uptake value (SUV) units using the formula SUV = [tissue activity concentration (Bq/cm³)/injected dose (Bq)] \times body weight (g). [¹⁸F]-FDG and ⁸⁹Zr uptake in the tumors was analyzed by drawing volumes of interest (VOI) manually containing the entire tumor, guided by CT when available. Semi-automatic segmentation was then performed including voxels with a value greater than 50% of the maximum value of the tumor. Finally, the average of the SUV values within the semi-automatic VOI was calculated (SUV mean).

Immunohistochemistry

Immunohistochemistry (IHC) was performed as previously described (13) using an antibody against *Id1* (1:1500, BCH-1/37-2; Biocheck, San Francisco, CA, USA). IHC was performed to study the expression of CD3 (1:150, ab16669; Abcam, Cambridge, United Kingdom), CD8 (1:400, #98941S; Cell Signaling, Danvers, MA, USA) and CD4 (1:400, #25229S; Cell Signaling, Danvers, MA, USA), as previously described (16). Slides were scanned using the Aperio Digital Scanner (Leica, Wetzlar, Germany) and analyzed with Image J software (NIH, Bethesda, MD, USA).

Multiplex-VECTRA

For multispectral immunophenotyping in mouse tumors, the murine-specific NEL810001KT Opal kit (Akoya, Marlborough, MA, USA) was used following the manufacturer's instructions and as previously described (16), with additional markers. This kit includes the Alexa Fluor tyramides Opals 520, 570 and 690 and spectral DAPI. Opals 650 (R55503) was not included in the kit, so was purchased separately from Akoya. The following primary antibodies were used: anti-CD3 (1:150, ab16669; Abcam, Cambridge, United Kingdom), anti-CD4 (1:200, #25229S; Cell Signaling, Danvers, MA, USA), anti-CD8 (1:400, #98941S; Cell Signaling, Danvers, MA, USA) and anti-*Id1* (1:1000, BCH-1/37-2; Biocheck, San Francisco, CA, USA). Vectra Polaris Automated Quantitative Pathology Imaging System and the Phenochart and InForm 2.4 software (Akoya, Marlborough, MA, USA) were used for sample scanning, spectral unmixing, and quantification of signals. Data were given as number of cells with a specific immunophenotype/total number of cells.

Statistical analysis

A Shapiro–Wilk test was conducted to analyze the normality of the samples. Statistical significance was assessed using a Mann–Whitney *U* test (for comparisons between two groups) and one-way ANOVA followed by a *post hoc* test, or Kruskal–Wallis followed by a *post hoc* test (for comparisons between different groups). The relationship between zirconium-89 uptake and immune cell infiltration was analyzed using Pearson correlations. A *p*-value of <0.05 was considered statistically significant. Statistical analyses were performed using Prism software version 8.0 (GraphPad, San Diego, CA, USA).

Results

[¹⁸F]-FDG-PET scan fails to identify PD-1/PD-L1 blockade antitumor response

In order to explore the limitations of conventional [¹⁸F]-FDG-PET scans for accurately assessing the response to immunotherapy treatments, we used a lung cancer syngeneic mouse model exposed to PD-1/PD-L1 axis blockade, as previously published (16).

We investigated the synergistic impact of anti-PD-1 treatment combined with *Id1* abrogation at the host tumor microenvironment. This therapeutic combination reduced LLC tumor growth. However, no statistically significant differences were observed between mice with constitutive expression of *Id1* (C57) and mice with *Id1* silenced at the host microenvironment (IDKO) (C57-LLC_Sc/PBS: 1709 [1171-2025]; C57-LLC_Sc/anti-PD-1: 1079 [489.5-1911]; IDKO-LLC_Sc/PBS: 874.2 [275.7-1473]; IDKO-LLC_Sc/anti-PD-1: 246.2) (Supplementary Figures S1A, B). In contrast with tumor volume, [¹⁸F]-FDG uptake did not show any significant tumor metabolic response (C57-LLC_Sc/PBS: 1.111 [0.894-1.405]; C57-LLC_Sc/anti-PD-1: 0.997 [0.715-1.404]; IDKO-LLC_Sc/PBS: 0.992 [0.541-1.409]; IDKO-LLC_Sc/anti-PD-1: 0.505 [0.311-0.680]) (Figures 1A, B).

We also studied the impact of anti-PD-1 blockade after complete inhibition of *Id1* expression (tumor cells and host microenvironment). *Id1* silencing (alone or in combination with anti-PD-1 therapy) significantly reduced tumor growth (C57-LLC_shID1/PBS: 947.6 [540.3-1334]; C57-LLC_shID1/PD-1: 1255 [1130-1359]; IDKO-LLC_shID1/PBS: 312.9 [30.07-596.7]; IDKO-LLC_shID1/PD-1: 47.09 [10.96-100.3], and *p*-values for the groups were as follows: C57-PBS/IDKO-PBS *p* = 0.0352; C57-PBS/IDKO-PD-1 *p* = 0.0066; C57-PD-1/IDKO-PBS *p* = 0.0027; C57-PD-1/IDKO-PD-1 *p* = 0.0007) (Supplementary Figures S1C, D). Of note, no significant differences [¹⁸F]-FDG uptake were observed among the different mice groups (C57-LLC_shID1/PBS: 1.8 [1.393-2.187]; C57-LLC_shID1/anti-PD-1: 1 [0.904-1.179]; IDKO-LLC_shID1/PBS: 1.3 [0.972-1.857]; IDKO-LLC_shID1/anti-PD-1: 1.3 [0.799-2.222]) (Figures 1C, D).

Taken together, these results suggest that the [¹⁸F]-FDG-PET scan fails to assess antitumor immune response upon PD-1/PD-L1 blockade in this animal model.

[⁸⁹Zr]-anti-PD-1 uptake correlates with tumor-infiltrating CD8⁺ T cells

Given the limitations observed with conventional [¹⁸F]-FDG-PET to monitor PD-1/PD-L1 blockade antitumor response, we used an additional novel radiotracer labeling protocol based on the use of anti-PD-1 mAb with ⁸⁹Zr. PD-L1 is widely expressed in both immune cells, as well as in tumor cells, whereas PD-1 is mainly expressed on the surface of activated T cells, B cells, and monocytes (25). Therefore, we hypothesized that [⁸⁹Zr]-anti-PD-1 signal may predict and correlate with tumor infiltrating lymphocytes.

Anti-PD-1 treated mice, in their last treatment dose, received an anti-PD-1 mAb labelled with ⁸⁹Zr, and the ⁸⁹Zr signal was sequentially measured by immuno-PET (Figure 2A). ⁸⁹Zr uptake was significantly higher in mouse tumors when *Id1* was inhibited at both the host microenvironment and tumor cells. Interestingly, this uptake was sustained until the end point of the experiment; (*p*-values for the groups were as follows: Day 15, C57 LLC_Sc *p* = 0.0133; C57 LLC_sh-ID1 *p* = 0.0032; Day 17, C57 LLC_Sc *p* = 0.0075; C57 LLC_sh-ID1 *p* = 0.0069; Day 20, C57 LLC_Sc *p* = 0.0002; C57 LLC_sh-ID1 *p* = 0.0001; IDKO LLC_Sc *p* = 0.0102) (Figures 2B, C; Table 1).

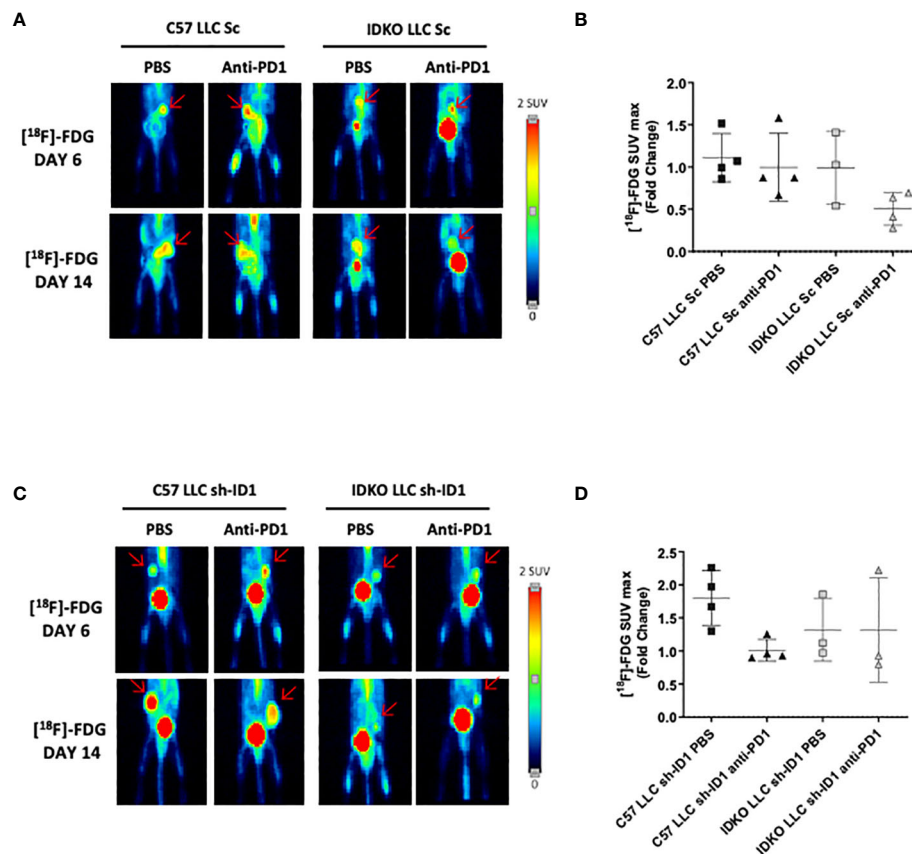


FIGURE 1

^{18}F -FDG does not detect the antitumor effect of PD-1 blockade in LLC tumors. (A) Representative PET images at days 6 and 13 of ^{18}F -FDG uptake in LLC cells (LLC Sc) injected in $Id1^{+/+}$ (C57BL/6J) or $Id1^{-/-}$ (IDKO) ($n = 4$) mice groups. (B) Quantification of ^{18}F -FDG SUVmax representing the fold change between the uptake at days 6 and 13 of the four mice groups described in (A). (C) Representative PET images of ^{18}F -FDG uptake at days 6 and 13 of $Id1$ silenced LLC cells (LLC sh-ID1) injected in $Id1^{+/+}$ (C57BL/6J) or $Id1^{-/-}$ (IDKO) ($n = 4$) mice groups. (D) Quantification of ^{18}F -FDG SUVmax representing the fold change between the uptake at days 6 and 13 of the four mice groups described in (C). Error bars denote SD.

The immune populations in tumor samples were then characterized. $Id1$ blockade in the tumor microenvironment ($Id1^{-/-}$ mice) significantly enhanced $\text{CD}3^+$ T cell infiltration in tumor samples as compared to $Id1^{+/+}$ mice. However, no significant differences were observed when additional $Id1$ genetic silencing in LLC cells was added to $Id1$ inhibition in the tumor microenvironment in terms of $\text{CD}3^+$ T cells infiltration in tumor samples; ($p > 0.0001$) (Figures 3A, B; Supplementary Figure S2A; Table 2). Similarly, the effector $\text{CD}8^+$ T cells tumor infiltration was significantly increased among $Id1$ -deficient animals as compared to $Id1$ -expressing mice. In contrast with the observations made regarding $\text{CD}3^+$ T cell infiltration, $\text{CD}8^+$ T cell infiltration was significantly higher in mice with complete $Id1$ depletion (tumor cells plus tumor microenvironment) ($p > 0.0001$; IDKO LLC_Sc/sh-ID1 $p = 0.0497$) (Figures 3A, B; Supplementary Figure S2B; Table 2). $Id1$ abrogation also enhanced infiltration of $\text{CD}4^+$ T cells ($p = 0.0488$) (Figures 3A, B; Supplementary Figure S2C; Table 2). Interestingly, a correlation was found between ^{89}Zr -anti-PD-1 uptake signal detected with immuno-PET and the presence of $\text{CD}3^+$ ($Cor = 0.8098$; $p = 0.0014$) and $\text{CD}8^+$ T cells ($Cor = 0.8035$; $p = 0.0016$) analyzed in tumor samples by IHC (Figure 3C).

Collectively, the Zr uptake and its correlation with TILs in anti-PD-1 responder mice, suggest that ^{89}Zr -anti-PD-1 immuno-PET allows an accurate evaluation of tumor response to immunotherapy.

$Id1$ abrogation enhanced proinflammatory interleukins expression

In order to explore the clinical relevance of $Id1$ depletion at the tumor microenvironment, we analyzed immune populations in tumors from mice responding to anti-PD-1 therapy (in $Id1$ -silenced host microenvironment) and non-responding mice (mice with constitutive $Id1$ expression). $Id1$ absence in the tumor microenvironment in $Id1$ -deficient mice significantly increased the tumor infiltration of $\text{CD}3^+$ T cells, and more importantly, effector $\text{CD}8^+$ T cells, as compared to $Id1$ -expressing mice ($\text{CD}3^+$ T cells $p > 0.0001$; $\text{CD}8^+$ T cells $p > 0.0001$) (Figures 4A, B; Table 3). Additionally, quantitative multiplexed IHC (labelling CD3, CD8 and $Id1$) revealed an increase in the proportion of $\text{CD}3^+$ TILs and $\text{CD}8^+$ T lymphocytes in tumors derived from $Id1$ knockout mice

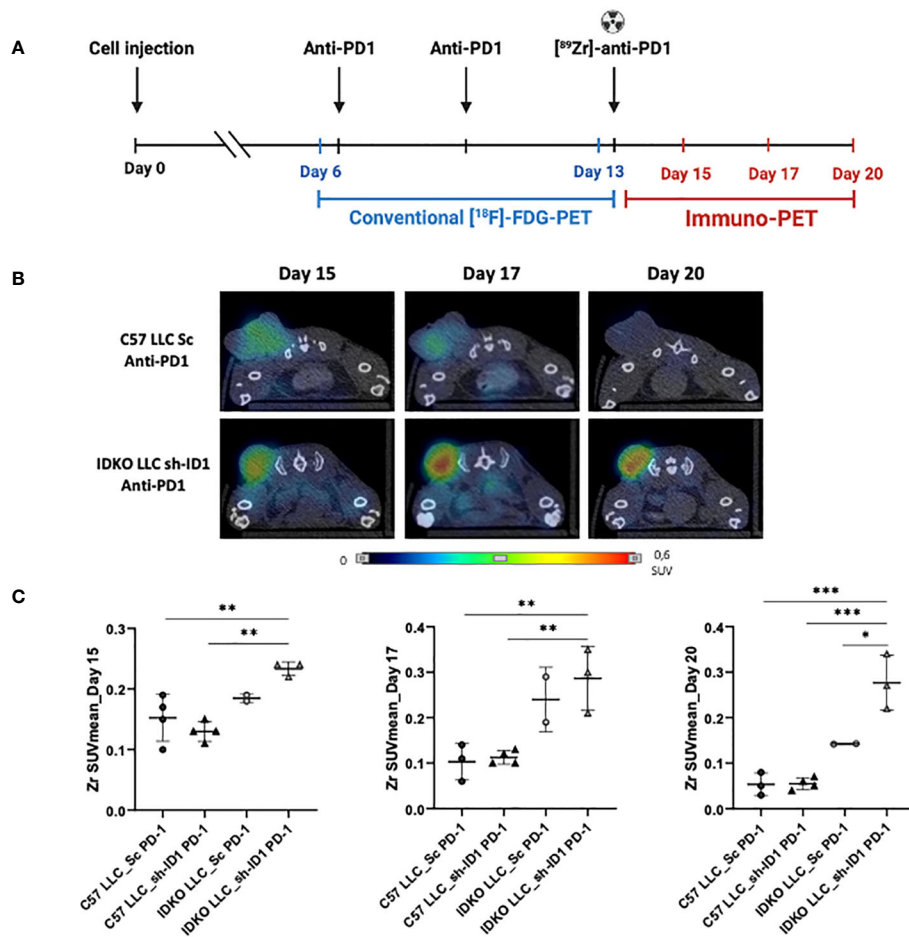


FIGURE 2 ^[89Zr]-anti-PD-1 allows an accurate evaluation of tumor response to immunotherapy in a lung cancer mouse model. (A) Outline of the mouse model. LLC [sh_Control (Sc) and *Id1* silenced cells (sh-ID1)] were subcutaneously injected in *Id1*^{+/+} C57BL/6J (C57) and *Id1*^{-/-} C57BL/6J (IDKO) mice, and animals were treated with PBS or an anti-PD-1 mAb (days 7, 10; RPM-14 100mg, intraperitoneally) and with ^[89Zr]-anti-PD-1 (day 14; 100mg, intraperitoneally) (n=4 mice per group). Tumor volume was measured using a caliper (mm³), using ^[18F]-FDG-PET scan analyses (days 6 and 13) or using ^[89Zr]-anti-PD-1 PET scans analysis (days 15, 17 and 20 after LLC inoculation). (B) Representative PET-CT images of ⁸⁹Zr signal at days 15, 17 and 20 after LLC inoculation. (C) ⁸⁹Zr signal LLC Sc and sh-ID1 cells injected in C57 and IDKO treated with anti-PD-1 at days 15, 17, and 20 after LLC inoculation. Asterisks denote significance (**p* < 0.05, ***p* < 0.005, ****p* < 0.001), and error bars denote SD.

(CD3⁺ T cells *p* = 0.0011; CD8⁺ T cells *p* > 0.0001) (Figures 4C, D; Table 3).

We also explored the expression of the cytokines *Il-1β*, *Tnf-α* and *Ifn-γ* using RT-PCR. *Id1* absence in the host microenvironment enhanced the expression of *Il-1b*, *Ifn-γ* and *Tnf-α*, factors implicated in immune T cell activation (*Il-1b*, C57: 0.28 [0.078-0.54]; IDKO: 0.95 [0.5-1.45], *p* > 0.0001; *Ifn-γ*: C57: 0.002 [0.0004-0.003]; IDKO:

0.033 [0.017-0.047], *p* > 0.0001; *Tnf-α*, C57: 0.005 [0.002-0.007]; IDKO: 0.06 [0.029-0.093], *p* = 0.0002) (Figure 4E).

Collectively, these data show that *Id1* absence in the host microenvironment can induce tumor TIL infiltration. More importantly, we also demonstrate that *Id1* inhibition may enhance proinflammatory interleukin expression implicated in immune T cell activation.

TABLE 1 ^[89Zr]-anti-PD-1 uptake from all mice treated with ^[89Zr]-anti-PD-1 at days 15, 17 and 20 after cell inoculation.

^[89Zr] -anti-PD-1 uptake (Day)	C57 LLC_Sc		C57 LLC_sh-ID1		IDKO LLC_Sc		IDKO LLC_sh-ID1	
	Mean	Interquartile range	Mean	Interquartile range	Mean	Interquartile range	Mean	Interquartile range
15	0.1467	0.1-0.19	0.13	0.115-0.145	0.185	0.18-0.19	0.2333	0.22-0.24
17	0.1033	0.06-0.14	0.1125	0.1-0.1275	0.24	0.19-0.29	0.2867	0.21-0.35
20	0.0533	0.03-0.08	0.055	0.0425-0.0675	0.1524	0.142-0.143	0.2767	0.22-0.34

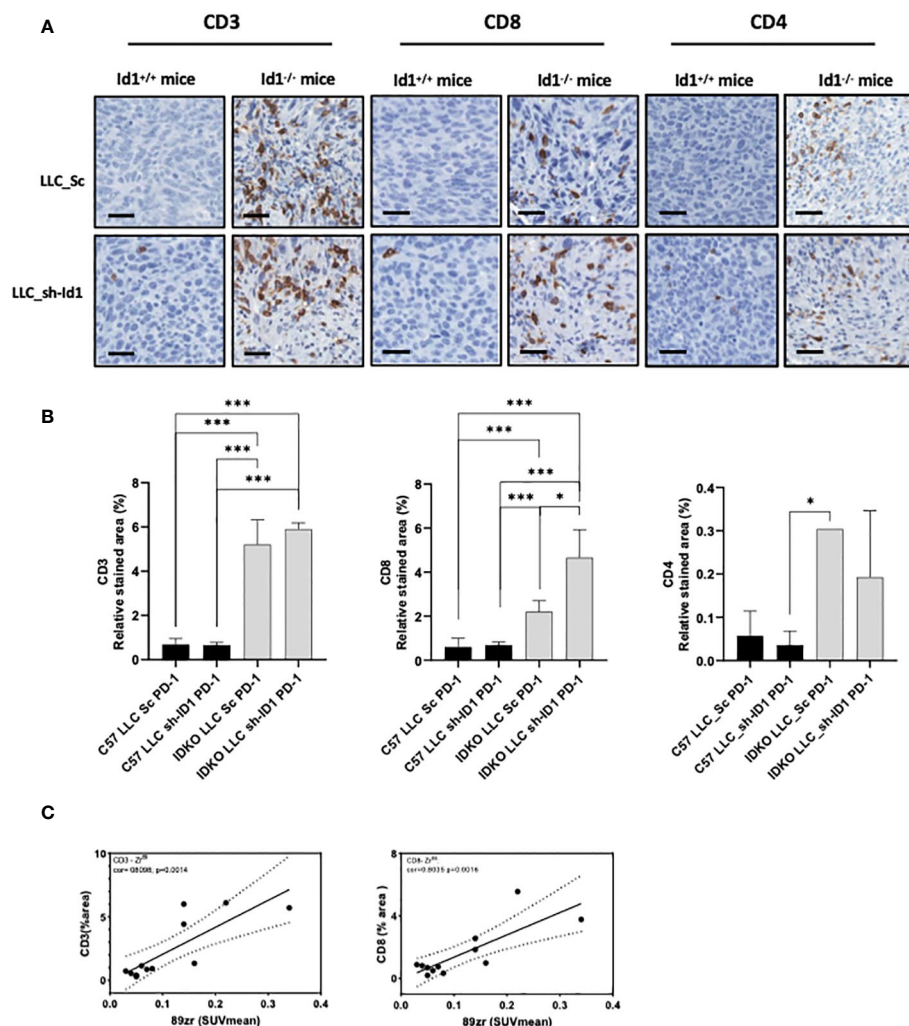


FIGURE 3 [⁸⁹Zr]-anti-PD-1 uptake correlates with immune T cell infiltration. (A) Representative IHC images illustrating: Left: CD3⁺ T cells; Middle: CD8⁺ T cells; Right: CD4⁺ T cells; Scale bar: 200μm. (B) Quantification of the relative stained area of: Left: CD3⁺ T cells; Middle: CD8⁺ T cells; Right: CD4⁺ T cells. (C) Correlation between ⁸⁹Zr uptake at day 20 after LLC inoculation and: Left: CD3⁺ T cells proportion area (Cor = 0.8); Right: CD8⁺ T cells proportion area (Cor = 0.8). Asterisks denote significance (*p < 0.05, ***p < 0.001), and error bars denote SD.

Discussion

Tumor response assessment has become a challenge in NSCLC patients receiving immunotherapy-based systemic regimens. According to their particular mechanisms of action based on T-cell activation, response to ICIs is characterized by different patterns, such as progression prior to treatment response

(pseudoprogression), hyperprogression, and dissociated responses following treatment. These patterns, however, are not reflected in the Response Evaluation Criteria in Solid Tumors version 1.1 (RECIST 1.1), which is the standard for response assessment in oncology. Therefore, new response evaluation tools are required.

In this paper, we propose the use of a PET-CT scan based on an [⁸⁹Zr]-anti-PD-1 radiotracer as a strategy to overcome the

TABLE 2 Immunohistochemical analysis of markers of tumor-infiltrating lymphocytes from all mice treated with [⁸⁹Zr]-anti-PD-1.

IHC marker	C57 LLC_Sc [⁸⁹ Zr]-anti-PD-1		C57 LLC_sh-ID1 [⁸⁹ Zr]-anti-PD-1		IDKO LLC_Sc [⁸⁹ Zr]-anti-PD-1		IDKO LLC_sh-ID1 [⁸⁹ Zr]-anti-PD-1	
	Median	Interquartile range	Median	Interquartile range	Median	Interquartile range	Median	Interquartile range
CD3	0.8551	0.228-1.482	0.659	0.463-0.855	5.209	-4.831-15.25	5.906	3.395-8.418
CD8	0.603	-0.024-1.229	0.692	0.478-0.906	2.202	-2.298-6.703	4.666	-6.681-16.01
CD4	0.057	-0.033-0.148	0.036	-0.016-0.087	0.304		0.193	-1.186-1.572

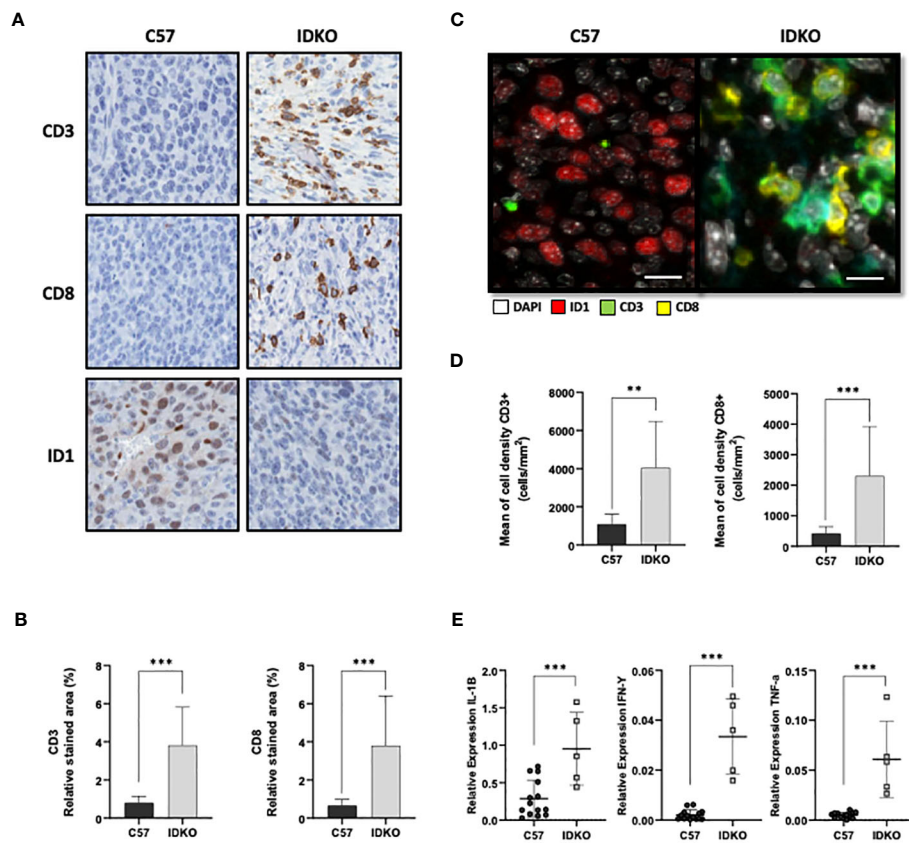


FIGURE 4 *Id1* inhibition at the tumor-microenvironment promotes proinflammatory interleukin expression and T cell infiltration. **(A)** Representative IHC images illustrating CD3⁺ T cells, CD8⁺ T cells and Id1⁺ cells of LLC cells inoculated in C57 and IDKO mice. Scale bar: 200µm. **(B)** Left: Quantification of proportion of relative stained area of CD3⁺ T cells. Right: Quantification of the proportion of relative stained area of CD8⁺ T cells of tumor samples illustrated in **(A)**. **(C)** Representative images of multiplex immunofluorescence staining panel with nuclei (white), Id1 (red), CD3 (green), CD8 (yellow) of LLC cells inoculated in C57 and IDKO mice. Scale bar: 200µm. **(D)** Left: Quantification of multiplex immunofluorescence staining of CD3⁺ T cells. Right: Quantification of multiplex immunofluorescence staining of CD8⁺ T cells of tumor samples illustrated in **(C)**. **(E)** Relative mRNA expression levels of *Il-1b*, *Ifn-γ* and *Tnf-α* in LLC tumors in C57 and IDKO mice. Asterisks denote significance (**p* < 0.05, ****p* < 0.001), and error bars denote SD.

limitations of conventional [¹⁸F]-FDG-PET scans in assessing immunotherapy antitumor responses. Our results show that an [⁸⁹Zr]-anti-PD-1-PET-CT could accurately assess tumor response to ICIs and may constitute a potential biomarker which directly labels effector T cells and predicts the efficacy of PD-1 inhibition in real time, non-invasively and safely.

[¹⁸F]-FDG-PET-CT is a powerful tool for monitoring lung cancer initial staging and antitumor response due to its ability to detect small metastatic lesions and regional lymph node tumor

spread more accurately than the conventional CT and MRI imaging methods (26, 27). A number of clinical studies have shown that alterations in metabolic activity, expressed as changes in SUV during induction therapy or at interim evaluation, are associated with tumor response. In NSCLC, a reduction of SUVmax below 2.5 after 2-4 conventional chemotherapy cycles has been considered a predictor of future response associated with a substantially higher median time to recurrence (28). Similarly, when the treatment studied is a targeted therapy, such as the EGFR tyrosine-kinase

TABLE 3 Immunohistochemical and multispectral immunophenotyping analysis of markers of tumor-infiltrating lymphocytes from anti-PD-1 non-responding and responding mice.

IHC marker	IHC				Multiplex-IHC			
	C57		IDKO		C57		IDKO	
	Mean	Interquartile range	Mean	Interquartile range	Mean	Interquartile range	Mean	Interquartile range
CD3	0.793	0.55-0.97	3.817	1.63-5.854	1075	542.3-1636	4053	1973-6500
CD8	0.656	0.385-0.866	3.803	1.934-5.112	441.2	246.3-549.7	2228	1162-3935

Immunohistochemical (IHC); multispectral immunophenotyping (Multiplex-IHC); anti-PD-1 non-responding mice (C57); anti-PD-1 responding mice (IDKO).

inhibitor erlotinib, a reduction in SUVmax measured by [^{18}F]-FDG-PET is also clearly associated with durable therapeutic responses in NSCLC patients (29). In contrast with conventional chemotherapy or targeted therapies, the response pattern of patients treated with ICIs may be substantially different, with some patients developing hyperprogression or pseudoprogression (30). [^{18}F]-FDG is a reliable radiotracer for monitoring glucose metabolism. However, changes in glucose metabolism are not restricted to tumor cells, and anti-tumor immune-related cells can similarly show major changes in the glucose metabolism when they are externally activated. ICIs reactivate effector T cells, boosting immune and natural inflammatory response and conventional [^{18}F]-FDG-PET scans have shown inaccuracies when examining responses to these drugs (31). We also observed limitations with [^{18}F]-FDG-PET in our lung cancer murine model when assessing tumor response to PD-1/PD-L1 axis blockade among mice responding to anti-PD-1 blockade and *Id1* inhibition. In previous studies, we have shown that *Id1* complete abrogation at both host microenvironment and tumor cells sensitized lung tumors to anti-PD-1 therapy, substantially reducing tumor growth (16). However, no significant differences were observed at the SUVmax [^{18}F]-FDG uptake level between responders and non-responders to immunotherapy.

According to RECIST, the tumor burden may transiently increase and then decrease as treatment continues, due to an immune reaction between tumor cells and host immune cells (32). The immune-related Response Evaluation Criteria in Solid Tumor (irRECIST) has been proposed as an update to the RECIST criteria for the assessment of response to ICIs (33). For PET response evaluation, different response criteria have also been proposed, such as the EORTC (European Organisation for Research and Treatment of Cancer) and PERCIST (Positron Emission Tomography Response Criteria in Solid Tumors) (34, 35). Nevertheless, the specific mechanism of action of ICIs has created unique [^{18}F]-FDG-PET-CT response patterns, which make it difficult to determine these responses using the PERCIST criteria. This has led to the elaboration of new multiple criteria specifically addressing ICIs response, such as PECRIT (Early Prediction of Response to Immune Checkpoint Inhibitor Therapy) or PERCIMT (Response Evaluation Criteria for Immunotherapy) (36). However, the lack of harmonization hampers the wider adoption of molecular imaging as a more accurate and reliable tool for response assessment to immune-modulating agents in cancer patients.

Immuno-PET is a whole-body, non-invasive molecular imaging technique that combines the high resolution, quantitative ability and sensitivity of PET with the specific binding property of mAbs (37). Immuno-PET has become a relevant novel imaging tool in the molecular evaluation of hematological malignancies and solid tumors (22, 37). Two approaches have been made to date using radiolabeled immunotherapy mAbs (pembrolizumab, nivolumab) and probes directed to target immune biomarkers (PD-1/PD-L1, CD8) (38–40). In NSCLC, [^{89}Zr]-nivolumab and [^{18}F]-BMS-986192 were studied in 13 patients. The median [^{18}F]-BMS-986192 and [^{89}Zr]-nivolumab SUVpeak was higher for lesions with $\geq 50\%$ tumor PD-L1 than for lesions with $< 50\%$ expression (8.2 vs. 2.9, $p = 0.018$); and aggregates of PD-1 positive tumor-

infiltrating immune cells (7.0 vs. 2.7, $p = 0.03$) (38). More recently, another study was performed in 12 NSCLC patients using [^{89}Zr]-pembrolizumab immuno-PET before pembrolizumab monotherapy. This study showed that [^{89}Zr]-pembrolizumab PET-CT is a safe and feasible imaging modality. Moreover, [^{89}Zr]-pembrolizumab uptake was higher among responding patients than non-responding patients, although no significant differences were observed (SUVpeak 11.4 vs 5.7, $p = 0.066$) (40). The NCT02760225 clinical trial, has recently evaluated the use of [^{89}Zr]-pembrolizumab to assess tumor uptake, antibody biodistribution and patient outcome in patients with locally advanced or metastatic melanoma and NSCLC. Interestingly, they found that [^{89}Zr]-pembrolizumab uptake not only correlated with response to anti-PD-1 therapy ($p = 0.014$), but also with progression-free survival (PFS) ($p = 0.0025$) and overall survival (OS) ($p = 0.026$) (23). More recently, a study performed in patients with head and neck squamous cell carcinoma and NSCLC showed [^{89}Zr]-BI 754111, a LAG-3 targeting mAb, to be a predictive imaging biomarker for anti-LAG-3 therapy (21).

Similarly, in our lung cancer mouse model we show that [^{89}Zr]-anti-PD-1 uptake in tumor lesions was significantly higher among treatment-responding *Id1* knock-out mice, than among non-responding mice maintaining a constitutive *Id1* expression. More importantly, the novelty of our study relies on the demonstration of a clear correlation between that [^{89}Zr]-anti-PD-1 uptake and the proportion of TILs (CD3^+ T and effector CD8^+ T cells) infiltrating tumor lesions and with a proinflammatory tumor microenvironment. As we previously demonstrated, *Id1* and PD-1 combine blockade synergy was generated mainly through CD8^+ T cells infiltration (16). We also showed in our mouse model an increase in the presence of CD8^+ T cells and the correlation with the [^{89}Zr]-anti-PD-1 uptake in anti-PD-1 responder mice. Consistently, we found a significant upregulation of proinflammatory cytokines in responding mice, such as *Ifn- γ* and *Tnf- α* , that are involved in CD8^+ T cell tumor killing activity (41, 42). Moreover, the expression of *Ifn- γ* and *Il-1 β* in tumor samples of anti-PD-1 responder mice, might suggest the infiltration by other antitumor immune system cells (43, 44). Therefore, taken together these data we provide a potential mechanistic explanation for the enhanced tumor response observed.

The main limitation of our study is the relatively small tumor sample size analyzed, since most mice with combined complete *Id1* genetic abrogation (*Id1*-deficient mice injected with *Id1*-silenced tumor cells) and PD-1 blockade showed complete regression of their syngeneic lung cancer tumors, so they could not be measured. Moreover, our experiments were only performed in immunologically competent murine models, so these results should be confirmed in humanized murine models.

We have demonstrated the utility of [^{89}Zr]-anti-PD-1 immuno-PET as a novel imaging tool for the non-invasive, real-time detection of antitumor effector TILs in a lung cancer mouse model responder to anti-PD-1 therapy. In this regard, [^{89}Zr]-anti-PD-1 (immuno-PET) may probably perform similarly well in other lung cancer subtypes for which immunotherapy has been approved in frontline treatment or as subsequent lines (*KRAS* or *BRAF* mutant lung tumors).

Conclusions

This study proposes the potential use of [⁸⁹Zr]-anti-PD-1 immuno-PET as a safe and feasible imaging modality to monitor PD-1/PD-L1 inhibitor antitumor response in NSCLC. We show that [⁸⁹Zr]-anti-PD-1 uptake is significantly higher in anti-PD-1-responding mice as compared to non-responding mice. Moreover, our data may confirm the capacity of [⁸⁹Zr]-anti-PD-1 immuno-PET to label PD-expressing immune cells, such as effector CD8⁺ TILs. Nevertheless, further investigation is warranted.

Data availability statement

The raw data supporting the conclusions of this article will be made available by the authors, without undue reservation.

Ethics statement

The animal study was approved by Committee on Animal Research and Ethics (regional Government of Navarra). The study was conducted in accordance with the local legislation and institutional requirements.

Author contributions

AP: Formal Analysis, Investigation, Methodology, Validation, Visualization, Writing – original draft, Writing – review & editing. MR-R: Formal Analysis, Investigation, Validation, Visualization, Writing – original draft, Writing – review & editing. IL: Data curation, Validation, Visualization, Writing – review & editing. FI: Formal Analysis, Writing – review & editing. JS: Writing – review & editing. ME: Data curation, Writing – review & editing. MC: Data curation, Formal Analysis, Writing – review & editing. AV-L: Formal Analysis, Writing – review & editing. AF-C: Data curation, Formal Analysis, Writing – review & editing. JS: Data curation, Formal Analysis, Writing – review & editing. SS: Writing – review & editing, Project administration, Supervision. IP: Project administration, Supervision, Writing – review & editing. AC: Project administration, Supervision, Writing – review & editing. DA: Project administration, Supervision, Writing – review & editing. IG-B: Conceptualization, Funding acquisition, Project administration, Supervision, Writing – original draft, Writing – review & editing.

Funding

AP was supported by Fundación Persán and Ayudas predoctorales para la realización de programas de doctorado de interés para Navarra 2021 fellowships. MRR was supported by a

donation from the family of José Luis Larrea. DA, and IGB were supported by a grant (RD12/0036/0040) from Red Temática de Investigación Cooperativa en Cáncer, Instituto de Salud Carlos III, Spanish Ministry of Economy and Competitiveness & European Regional Development Fund “Una manera de hacer Europa” (FEDER; PI17/00411). IGB was also supported by two grants from Instituto de Salud Carlos III (PI15/02223 and PI19/00678), two grants from the Gobierno de Navarra cofunded by the Fondo Europeo de Desarrollo Regional 2014-2020 of Navarra (44/2017 and 53/2021). DA was also supported by the Fundación Científica de la Asociación Española Contra el Cáncer (IDEAS211016AJON), Gobierno de Navarra cofunded by the Fondo Europeo de Desarrollo Regional 2014-2020 of Navarra (51-2021), and Fondo de Investigación Sanitaria-Fondo Europeo de Desarrollo Regional Una manera de hacer Europa (PI20/00419). This study has received a grant for medical writing and article editing from Sociedad Española de Oncología (SEOM). The author(s) declare financial support was received for the research, authorship, and/or publication of this article.

Acknowledgments

We express our gratitude to Cristina Sainz and Miriam Redrado (CIMA) for technical help in the analysis of multiplex immunophenotyping.

Conflict of interest

The authors declare that the research was conducted in the absence of any commercial or financial relationships that could be construed as a potential conflict of interest.

The author(s) declared that they were an editorial board member of *Frontiers*, at the time of submission. This had no impact on the peer review process and the final decision.

Publisher's note

All claims expressed in this article are solely those of the authors and do not necessarily represent those of their affiliated organizations, or those of the publisher, the editors and the reviewers. Any product that may be evaluated in this article, or claim that may be made by its manufacturer, is not guaranteed or endorsed by the publisher.

Supplementary material

The Supplementary Material for this article can be found online at: <https://www.frontiersin.org/articles/10.3389/fimmu.2023.1272570/full#supplementary-material>

References

- Siegel RL, Miller KD, Wagle NS, Jemal A. Cancer statistics, 2023. *CA Cancer J Clin* (2023) 73:17–48. doi: 10.3322/caac.21763
- Chaft JE, Rimmer A, Weder W, Azzoli CG, Kris MG, Cascone T. Evolution of systemic therapy for stages I-III non-metastatic non-small-cell lung cancer. *Nat Rev Clin Oncol* (2021) 18:547–57. doi: 10.1038/s41571-021-00501-4
- Król K, Mazur A, Stachyra-Strawa P, Grzybowska-Szatkowska L. Non-small cell lung cancer treatment with molecularly targeted therapy and concurrent radiotherapy-A review. *Int J Mol Sci* (2023) 24:5858. doi: 10.3390/ijms24065858
- Rodríguez-Abreu D, Powell SF, Hochmair MJ, Gadgeel S, Esteban E, Felip E, et al. Pemetrexed plus platinum with or without pembrolizumab in patients with previously untreated metastatic nonsquamous NSCLC: protocol-specified final analysis from KEYNOTE-189. *Ann Oncol* (2021) 32:881–95. doi: 10.1016/j.annonc.2021.04.008
- Havel JJ, Chowell D, Chan TA. The evolving landscape of biomarkers for checkpoint inhibitor immunotherapy. *Nat Rev Cancer* (2019) 19:133–50. doi: 10.1038/s41568-019-0116-x
- Grant MJ, Herbst RS, Goldberg SB. Selecting the optimal immunotherapy regimen in driver-negative metastatic NSCLC. *Nat Rev Clin Oncol* (2021) 18:625–44. doi: 10.1038/s41571-021-00520-1
- Kuske M, Westphal D, Wehner R, Schmitz M, Beissert S, Praetorius C, et al. Immunomodulatory effects of BRAF and MEK inhibitors: Implications for Melanoma therapy. *Pharmacol Res* (2018) 136:151–9. doi: 10.1016/j.phrs.2018.08.019
- Doroshov DB, Sanmamed MF, Hastings K, Politi K, Rimm DL, Chen L, et al. Immunotherapy in non-small cell lung cancer: facts and hopes. *Clin Cancer Res* (2019) 25:4592–602. doi: 10.1158/1078-0432.CCR-18-1538
- Perk J, Iavarone A, Benezra R. Id family of helix-loop-helix proteins in cancer. *Nat Rev Cancer* (2005) 5:603–14. doi: 10.1038/nrc1673
- Lasorella A, Benezra R, Iavarone A. The ID proteins: master regulators of cancer stem cells and tumour aggressiveness. *Nat Rev Cancer* (2014) 14:77–91. doi: 10.1038/nrc3638
- Ponz-Sarvisé M, Nguwa PA, Pajares MJ, Agorreta J, Lozano MD, Redrado M, et al. Inhibitor of differentiation-1 as a novel prognostic factor in NSCLC patients with adenocarcinoma histology and its potential contribution to therapy resistance. *Clin Cancer Res* (2011) 17:4155–66. doi: 10.1158/1078-0432.CCR-10-3381
- Papaspyridonos M, Matei I, Huang Y, do Rosario Andre M, Brazier-Mitouart H, Waite JC, et al. Id1 suppresses anti-tumour immune responses and promotes tumour progression by impairing myeloid cell maturation. *Nat Commun* (2015) 6:6840. doi: 10.1038/ncomms7840
- Castañón E, Soltermann A, López I, Román M, Ecay M, Collantes M, et al. The inhibitor of differentiation-1 (Id1) enables lung cancer liver colonization through activation of an EMT program in tumor cells and establishment of the pre-metastatic niche. *Cancer Lett* (2017) 402:43–51. doi: 10.1016/j.canlet.2017.05.012
- Román M, López I, Guruceaga E, Baraibar I, Ecay M, Collantes M, et al. Inhibitor of differentiation-1 sustains mutant KRAS-driven progression, maintenance, and metastasis of lung adenocarcinoma via regulation of a FOSL1 network. *Cancer Res* (2019) 79:625–38. doi: 10.1158/0008-5472.CAN-18-1479
- Melief J, Pico de Coaña Y, Maas R, Fennemann F-L, Wolodarski M, Hansson J, et al. High expression of ID1 in monocytes is strongly associated with phenotypic and functional MDSC markers in advanced melanoma. *Cancer Immunol Immunother* (2020) 69:513–22. doi: 10.1007/s00262-019-02476-9
- Baraibar I, Roman M, Rodríguez-Remírez M, et al. Id1 and PD-1 combined blockade impairs tumor growth and survival of KRAS-mutant lung cancer by stimulating PD-L1 expression and tumor infiltrating CD8+ T cells. *Cancers (Basel)* (2020) 12:3169. doi: 10.3390/cancers12113169
- Gridelli C, Rossi A, Carbone DP, Guarize J, Karachaliou N, Mok T, et al. Non-small-cell lung cancer. *Nat Rev Dis Primers* (2015) 1:15009. doi: 10.1038/nrdp.2015.9
- Reck M, Rabe KF. Precision diagnosis and treatment for advanced non-small-cell lung cancer. *N Engl J Med* (2017) 377:849–61. doi: 10.1056/NEJMra1703413
- Sollini M, Cozzi L, Antunovic L, Chiti A, Kirienko M. PET Radiomics in NSCLC: state of the art and a proposal for harmonization of methodology. *Sci Rep* (2017) 7:358. doi: 10.1038/s41598-017-00426-y
- Aide N, Hicks RJ, Le Tourneau C, Lheureux S, Fanti S, Lopci E. FDG PET/CT for assessing tumour response to immunotherapy: report on the EANM symposium on immune modulation and recent review of the literature. *Eur J Nucl Med Mol Imaging* (2019) 46:238–50. doi: 10.1007/s00259-018-4171-4
- Miedema IHC, Huisman MC, Zwezerijnen GJC, Grempler R, Pitarch AP, Thiele A, et al. 89Zr-immuno-PET using the anti-LAG-3 tracer [89Zr]Zr-BI 754111: demonstrating target specific binding in NSCLC and HNSCC. *Eur J Nucl Med Mol Imaging* (2023) 50(7):2068–80. doi: 10.1007/s00259-023-06164-w
- Carmon KS, Azhdarinia A. Application of immuno-PET in antibody-drug conjugate development. *Mol Imaging* (2018) 17:1536012118801223. doi: 10.1177/1536012118801223
- Kok IC, Hooiveld JS, van de Donk PP, Giesen D, van der Veen EL, Lub-de Hooge MN, et al. 89Zr-pembrolizumab imaging as a non-invasive approach to assess clinical response to PD-1 blockade in cancer. *Ann Oncol* (2022) 33:80–8. doi: 10.1016/j.annonc.2021.10.213
- Vosjan MJWD, Perk LR, Visser GWM, Budde M, Jurek P, Kiefer GE, et al. Conjugation and radiolabeling of monoclonal antibodies with zirconium-89 for PET imaging using the bifunctional chelate p-isothiocyanatobenzyl-desferrioxamine. *Nat Protoc* (2010) 5:739–43. doi: 10.1038/nprot.2010.13
- Pauken KE, Torchia JA, Chaudhri A, Sharpe AH, Freeman GJ. Emerging concepts in PD-1 checkpoint biology. *Semin Immunol* (2021) 52:101480. doi: 10.1016/j.smim.2021.101480
- Kandathil A, Kay FU, Butt YM, Wachsmann JW, Subramaniam RM. Role of FDG PET/CT in the eighth edition of TNM staging of non-small cell lung cancer. *Radiographics* (2018) 38:2134–49. doi: 10.1148/rgr.2018180060
- Castello A, Rossi S, Lopci E. 18F-FDG PET/CT in restaging and evaluation of response to therapy in lung cancer: state of the art. *Curr Radiopharm* (2020) 13:228–37. doi: 10.2174/1874471013666191230144821
- Kim SH, Lee JH, Lee GJ, Jeong S, Kwak Y-K, Kim H-K, et al. Interpretation and prognostic value of positron emission tomography-computed tomography after induction chemotherapy with or without radiation in IIIA-N2 non-small cell lung cancer patients who receive curative surgery. *Med (Baltimore)* (2015) 94:e955. doi: 10.1097/MD.0000000000000955
- Cook GJR, O'Brien ME, Siddique M, Chicklore S, Loi HY, Sharma B, et al. Non-small cell lung cancer treated with erlotinib: heterogeneity of (18)F-FDG uptake at PET-association with treatment response and prognosis. *Radiology* (2015) 276:883–93. doi: 10.1148/radiol.2015141309
- Champiat S, Dercle L, Ammari S, Massard C, Hollebecq A, Postel-Vinay S, et al. Hyperprogressive disease is a new pattern of progression in cancer patients treated by anti-PD-1/PD-L1. *Clin Cancer Res* (2017) 23:1920–8. doi: 10.1158/1078-0432.CCR-16-1741
- Evangelista L, de Jong M, Del Vecchio S, Cai W. The new era of cancer immunotherapy: what can molecular imaging do to help? *Clin Transl Imaging* (2017) 5:299–301. doi: 10.1007/s40336-017-0241-z
- Won SE, Park HJ, Byun S, Pyo J, Kim JH, Choi C-M, et al. Impact of pseudoprogression and treatment beyond progression on outcome in patients with non-small cell lung cancer treated with immune checkpoint inhibitors. *Oncimmunology* (2020) 9:1776058. doi: 10.1080/2162402X.2020.1776058
- Seymour L, Bogaerts J, Perrone A, Ford R, Schwartz LH, Mandrekas S, et al. iRECIST: guidelines for response criteria for use in trials testing immunotherapeutics. *Lancet Oncol* (2017) 18:e143–52. doi: 10.1016/S1470-2045(17)30074-8
- Young H, Baum R, Cremerius U, Herholz K, Hoekstra O, Lammertsma AA, et al. Measurement of clinical and subclinical tumour response using [18F]-fluorodeoxyglucose and positron emission tomography: review and 1999 EORTC recommendations. European Organization for Research and Treatment of Cancer (EORTC) PET Study Group. *Eur J Cancer* (1999) 35:1773–82. doi: 10.1016/S0959-8049(99)00229-4
- Wahl RL, Jacene H, Kasamon Y, Lodge MA. From RECIST to PERCIST: Evolving Considerations for PET response criteria in solid tumors. *J Nucl Med* (2009) 50(Suppl 1):122S–50S. doi: 10.2967/jnumed.108.057307
- Léger M-A, Routy B, Juneau D. FDG PET/CT for evaluation of immunotherapy response in lung cancer patients. *Semin Nucl Med* (2022) 52:707–19. doi: 10.1053/j.semnuclmed.2022.04.010
- Triumbari EKA, Morland D, Laudicella R, Bauckneht M, Albano D, Annunziata S. Clinical applications of immuno-PET in lymphoma: a systematic review. *Cancers (Basel)* (2022) 14:3488. doi: 10.3390/cancers14143488
- Niemeijer AN, Leung D, Huisman MC, Bahce I, Hoekstra OS, van Dongen GMS, et al. Whole body PD-1 and PD-L1 positron emission tomography in patients with non-small-cell lung cancer. *Nat Commun* (2018) 9:4664. doi: 10.1038/s41467-018-07131-y
- Farwell MD, Gamache RF, Babazada H, Hellmann MD, Harding JJ, Korn R, et al. CD8-targeted PET imaging of tumor-infiltrating T cells in patients with cancer: A phase I first-in-humans study of 89Zr-df-IAB2M2C, a radiolabeled anti-CD8 minibody. *J Nucl Med* (2022) 63:720–6. doi: 10.2967/jnumed.121.262485
- Niemeijer A-LN, Oprea-Lager DE, Huisman MC, Hoekstra OS, Boellaard R, de Wit-van der Ven BJ, et al. Study of 89Zr-pembrolizumab PET/CT in patients with advanced-stage non-small cell lung cancer. *J Nucl Med* (2022) 63:362–7. doi: 10.2967/jnumed.121.261926
- Ajona D, Ortiz-Espinosa S, Moreno H, Lozano T, Pajares MJ, Agorreta J, et al. A combined PD-1/C5a blockade synergistically protects against lung cancer growth and metastasis. *Cancer Discov* (2017) 7:694–703. doi: 10.1158/2159-8290.CD-16-1184
- Valencia K, Echebare M, Teijeira A, Pasquier A, Bértolo C, Sainz C, et al. DSTYK inhibition increases the sensitivity of lung cancer cells to T cell-mediated cytotoxicity. *J Exp Med* (2022) 219:e20220726. doi: 10.1084/jem.20220726
- Luetke-Eversloh M, Cicek BB, Siracusa F, Thom JT, Hamann A, Frischbutter S, et al. NK cells gain higher IFN- γ competence during terminal differentiation. *Eur J Immunol* (2014) 44:2074–84. doi: 10.1002/eji.201344072
- Ahn S, Jeong D, Oh SJ, Ahn J, Lee SH, Chung DH. GM-CSF and IL-4 produced by NKT cells inversely regulate IL-1 β production by macrophages. *Immunol Lett* (2017) 182:50–6. doi: 10.1016/j.imlet.2017.01.003